Reverse gate leakage mechanism of AlGaN/GaN HEMTs with Au-free gate

Xin Jiang(蒋鑫)[1,2], Chen-Hao Li(李晨浩)[1,2], Shuo-Xiong Yang(羊硕雄)[2], Jia-Hao Liang(梁家豪)[2], Long-Kun Lai(来龙坤)[1,2], Qing-Yang Dong(董青杨)[1,2], Wei Huang(黄威)[2], Xin-Yu Liu(刘新宇)[1,2,†], and Wei-Jun Luo(罗卫军)[1,2,‡]

[1] *Institute of Microelectronics, Chinese Academy of Sciences, Beijing 100029, China*
[2] *University of Chinese Academy of Sciences, Beijing 100190, China*

(Received 1 June 2022; revised manuscript received 11 July 2022; accepted manuscript online 5 August 2022)

The reverse gate leakage mechanism of W-gate and TiN-gate AlGaN/GaN high-electron-mobility transistors (HEMTs) with N_2 plasma surface treatment is investigated using current–voltage (I–V) and capacitance–voltage (C–V) characteristics and theoretical calculation analysis. It is found that the main reverse gate leakage mechanism of both devices is the trap-assisted tunneling (TAT) mechanism in the entire reverse bias region (−30 V to 0 V). It is also found that the reverse gate leakage current of the W-gate AlGaN/GaN HEMTs is smaller than that of the TiN gate at high reverse gate bias voltage. Moreover, the activation energies of the extracted W-gate and TiN-gate AlGaN/GaN HEMTs are 0.0551 eV–0.127 eV and 0.112 eV–0.201 eV, respectively.

Keywords: AlGaN/GaN, trap-assisted tunneling (TAT), W gate, TiN gate

PACS: 72.80.Ey, 73.40.Qv, 85.30.–z, 73.20.–r **DOI:** 10.1088/1674-1056/ac8735

1. Introduction

AlGaN/GaN high-electron-mobility transistors (HEMTs) have great advantages in high-power switching, microwave amplifiers, and high-temperature integrated circuits (ICs)[1,2] because of their high electron mobility, high saturation speed, high breakdown electric field strength, and good thermal stability. In recent years, in order to realize the integration of GaN devices and silicon-based complementary metal-oxide-semiconductor (CMOS) chips and to reduce the cost of IC production and manufacturing, CMOS-compatible fabrication process for AlGaN/GaN HEMTs has been extensively studied.[3,4] For Si-CMOS processing line, an Au-free environment is required to meet the strict contamination rules. Therefore, the Au-free gate technology is required in the integration of GaN devices and CMOS chip. So far, researchers have tried many materials to replace Au-gate, such as W, WN, Pd, Pt, TaN, Ti, TiN, Ir, Cr, WSi, and WSiN.[5–8] Compared with other Au-free gate materials, TiN-gate and W-gate exhibit attractive advantages in work function (4.6 eV for W, 5 eV for TiN), compatibility to CMOS processes (such as dry etch, wet etch, and sputter), low cost, high thermally stability (both are $\sim$ 700 °C), and so on.[5,9]

However, large reverse gate leakage current is still a serious problem for Au-free gate AlGaN/GaN HEMTs, which will increase low-frequency noise, reduce power supply efficiency, cause current collapses effect, and reduce breakdown voltage.[10,11] Therefore, it is important to analyze and research reverse gate leakage current in Au-free gate AlGaN/GaN HEMTs. Soltani *et al.* reported that the TiN gate contact on AlGaN/GaN transistor shows low reverse leakage current with low trapping phenomena.[6] Li *et al.* reported that AlGaN/GaN HEMTs with TiN gate exhibit a comparable DC output and transfer performance compared to devices with traditional Ni/Au gate,[5] and also show enhanced OFF-state breakdown voltage. Li *et al.* analyzed the reverse gate leakage current mechanism of TiN gate AlGaN/GaN HEMTs, and found that the leakage mechanism in the low bias region is Pool–Frenkel emission (PF), and the leakage mechanism in the high reverse bias region is trap-assisted tunneling (TAT) emission.[12] However, Li *et al.* did not mention the method of surface treatment before the formation of Schottky contacts, which is very important for the reverse leakage mechanism because different surface treatment methods before forming Schottky contacts may cause different leakage mechanisms.[13,14] According to Refs. [13,15], N_2 plasma surface treatment can optimize the interface of AlGaN/GaN HEMTs Schottky contacts and reduce reverse leakage current. Therefore, it is necessary to study the reverse leakage mechanism for TiN gate AlGaN/GaN HEMTs with N_2 plasma. In literature, researchers[16,17] reported that W-gate GaN HEMTs show lower reverse leakage current compared to devices with Ni/Au/Ni and Ni gate. Kawanago *et al.* studied the effect on current collapse of W gate AlGaN/GaN HEMTs.[18] However,

†Corresponding author. E-mail: xyliu@ime.ac.cn
‡Corresponding author. E-mail: luoweijun@ime.ac.cn

© 2023 Chinese Physical Society and IOP Publishing Ltd

the reverse gate leakage mechanism of W-gate AlGaN/GaN HEMTs was ignored and has not been studied yet. Therefore, it is significant to study the reverse leakage mechanism of W gate AlGaN/GaN HEMTs. Research of the reverse leakage mechanism of TiN gate and W gate AlGaN/GaN HENMTs will also promote the development of Au-free gate AlGaN/GaN HENMTs.

In this paper, the mechanism of the reverse leakage current of W gate and TiN gate AlGaN/GaN HEMTs in wide ranges of reverse bias voltages (-30 V $< V_R < 0$ V) and temperature (273 K–473 K) is analyzed in detail. This paper is arranged as follows: In Section 2, the process flow of Au-free gate AlGaN/GaN HEMTs is introduced. In Section 3, we mainly discuss and analyze the current–voltage (I_G–V_G) characteristics of AlGaN/GaN HEMTs under different reverse biases and temperatures. Finally, the conclusions are drawn in Section 4.

2. Experiment

In this work, an epitaxial layer of AlGaN/GaN HEMTs was grown on a 3-inch sapphire substrate by metal chemical vapor deposition (MOCVD), where the epitaxial layer includes a 1-μm-thick GaN buffer layer, and a 22-nm-thick AlGaN barrier layer with Al mole fraction of 26%. The fabrication process, device structure, and device drawing are shown in Fig. 1. The process flow of AlGaN/GaN HEMTs includes ohmic contact metallization, and then it was annealed at 870 °C for 40 s under N_2 environment. The devices were isolated by implanting N^+ and the gate recess was etched by inductively coupled plasma. Before the Schottky gate was formed, we treated the gate recessed area in the same way: W-gate AlGaN/GaN HEMTs and TiN-gate AlGaN/GaN HEMTs were surface treated with N_2 (20 sccm) plasma with RF power of 15 W for 3 min at pressure of 3 Pa.[13] We used different metals to form Schottky contacts: for W-gate AlGaN/GaN HEMTs, the Schottky contact was formed by electron beam evaporation W (500 Å), while for TiN-gate AlGaN/GaN HEMTs, the Schottky contact was formed by sputtering TiN with a thickness of 500 Å. The gate length, source-to-drain spacing, and gate width of the two devices are 0.25 μm, 3.5 μm, and 60 μm, respectively. Finally, the Si_3N_4 passivation layer was deposited by plasma-enhanced chemical vapor phase deposition (PECVD). The Agilent B1500 was used to measure the I–V characteristics of the device under the conditions of 273 K–473 K in steps of 50 K, and then the capacitance–voltage (C–V) characteristics was measured at room temperature.[19]

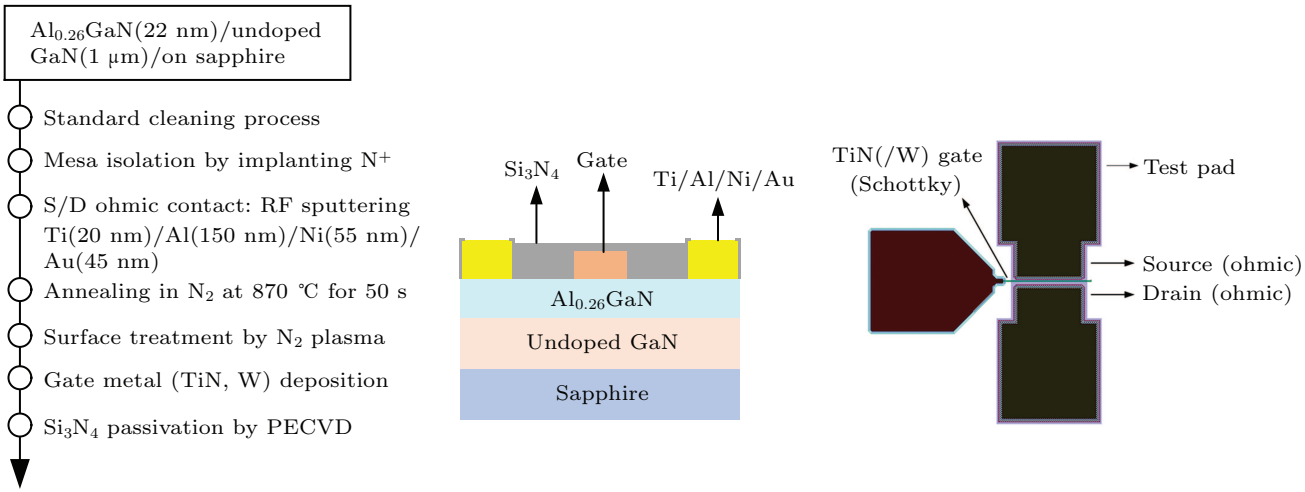


Fig. 1. Fabrication process, device structure, and device drawing for AlGaN/GaN HEMT.

3. Results and discussion

As shown in Fig. 2, the reverse gate leakage current of AlGaN/GaN HEMTs with different gate metals at 273 K–473 K was measured. It can be clearly seen from the figure that the reverse gate leakage current becomes larger as the reverse gate voltage increases, and the reverse gate leakage current also becomes larger as the temperature increases. Table 1 exhibits the current density of W-gate and TiN-gate AlGaN/GaN HEMTs at different reverse gate bias at 323 K. It is obvious that at the same temperature and gate voltage, the reverse leakage current of W-gate AlGaN/GaN HEMTs was smaller than that of TiN-gate AlGaN/GaN HEMTs at high reverse gate bias voltage. In order to study the reverse gate leakage mechanism of W-gate and TiN-gate AlGaN/GaN HEMTs, various reverse leakage current transport models will be compared to the measured data at low and high reverse gate biases.

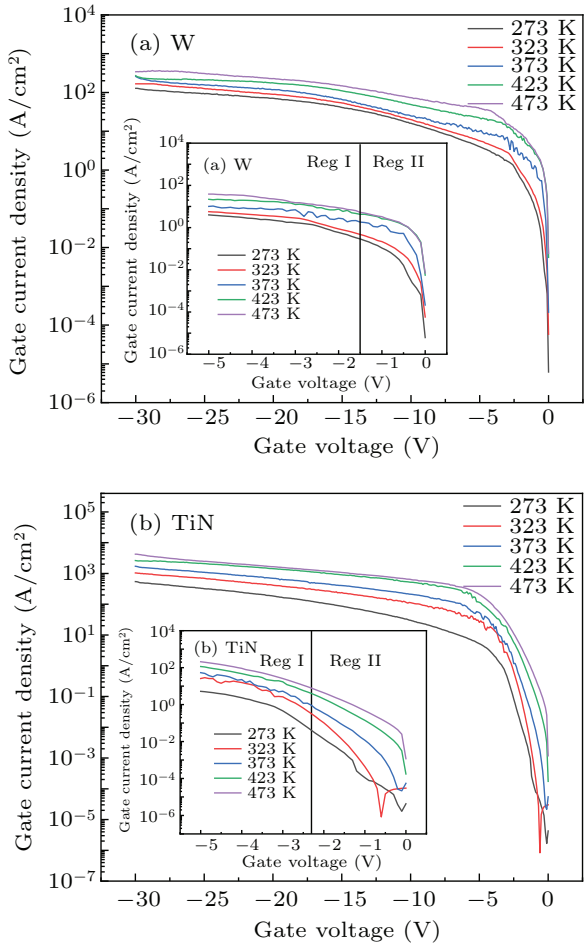


Fig. 2. Reverse gate current density-gate voltage characteristics of two samples at different temperatures: (a) W gate AlGaN HEMT, (b) TiN gate AlGaN HEMT.

Table 1. The current density (J_R) of W-gate and TiN-gate AlGaN/GaN HEMTs.

Voltage (V)	W gate J_R (A/cm^2)	TiN gate J_R (A/cm^2)
–1.0	0.2175	0.0004
–2.5	3.0070	0.6447
–3.0	2.8432	2.6258
–5	5.6873	25.7133
–15	53.5500	238.9667
–20	89.5267	414.6333
–25	125.2333	695.4000

3.1. Leakage current mechanisms at low reverse bias voltage

As shown in Fig. 2, at low reverse bias voltage (W-gate AlGaN/GaN HEMTs: in region Ⅱ, -1.5 V $< V_R < 0$ V; TiN-gate AlGaN/GaN HEMTs: in region Ⅱ, -2.3 V $< V_R < 0$ V). It can be clearly observed that the reverse leakage current becomes larger as the temperature rises, which is the same as the result reported by other researchers.[20,21] Temperature-dependent gate leakage mechanism,[22] such as thermionic emission (TE), Poole–Frenkel emission (PF), and TAT, will be used to analyze the reverse leakage current mechanism of W-gate and TiN-gate AlGaN/GaN HEMTs.

3.1.1. Thermionic emission current

Considering the leakage current in Au-free gate AlGaN/GaN HEMTs, for the thermionic emission mechanism, the carriers absorb the thermal energy and then emit over the potential barrier at the M–S interface. The J_R–V_R characteristics of thermionic emission are characterized by the expression[20]

$$J_R = A^* T^2 \exp\left[-\frac{q}{k_B T}\left(\varphi_B - \sqrt{\frac{qE}{4\pi\varepsilon_{s(h)}\varepsilon_0}}\right)\right], \tag{1}$$

where A^* refers to the effective Richardson's constant, T refers to the temperature, q refers to the electron charge, k_B refers to the Boltzmann's constant, ε_0 refers to the vacuum permittivity, $\varepsilon_{s(h)}$ refers to the high-frequency (optical) dielectric constant ($\varepsilon_{s(h)} = 5.2$) of $Al_{0.26}Ga_{0.74}N$.[23] $q\varphi_B$ refers to the Schottky barrier height and E refers to the electric field at the M–S interface, Eq. (1) can be rearranged as

$$\ln\left(\frac{J_R}{T^2}\right) = K_{TE}(T)\sqrt{E} + C_{TE}(T), \tag{2}$$

$$K_{TE}(T) = \frac{q}{2k_B T}\sqrt{\frac{q}{\pi\varepsilon_{s(h)}\varepsilon_0}}, \tag{3}$$

$$C_{TE}(T) = \frac{q\phi_B}{k_B T} + \ln A^*. \tag{4}$$

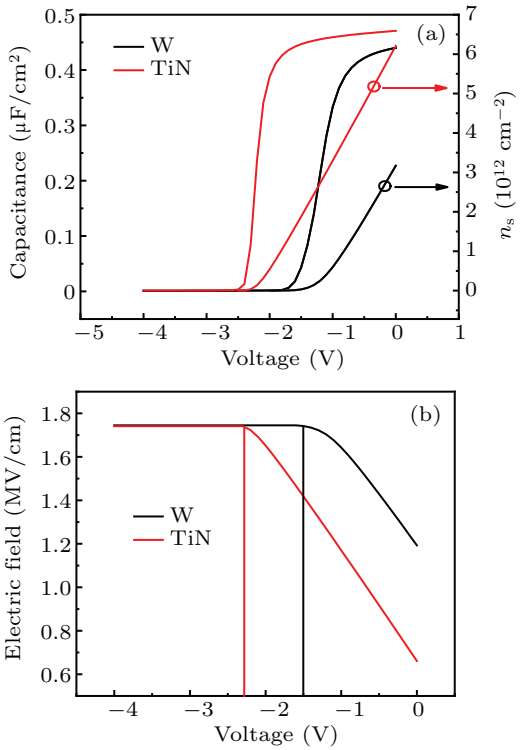


Fig. 3. (a) Capacitance–Voltage (C–V) characteristics; (b) the calculated electric field E vs. the voltage of the AlGaN/GaN HEMTs.

To calculate the near-surface electric field E underneath the Schottky contacts metal, a high-frequency (1 MHz) capacitance–voltage (C–V) scan is used to determine the n_s density at the AlGaN/GaN interface as a function of reverse

bias.[24] The C–V curves at room temperature (300 K) are described in Fig. 3. From the C–V characteristic curve, the extracted threshold voltages $V_{\rm Th}$ of W gate HEMTs and TiN gate HEMTs are -1.5 V and -2.3 V, respectively. It can be clearly seen that the threshold voltage of the W gate is much smaller than that of the TiN gate. The difference in threshold voltage is mainly due to the different work functions of TiN (~ 5 eV) and W (~ 4.5 eV). The $n_{\rm 2DEG}$ can be calculated by integration of the C–V characteristic curve from pinch-off voltage to 0 V. The electric field E across the barrier can be expressed as[25]

$$E = \frac{q(\sigma_{\rm p} - n_{\rm s})}{\varepsilon_0 \varepsilon_{\rm r}}, \tag{5}$$

where $\sigma_{\rm p}$ refers to the fixed polarization charge at hetero-interface, which is approximately equal to 1×10^{13} cm^2;[26] ε_0 refers to the vacuum permittivity, $\varepsilon_{\rm r}$ refers to the relative dielectric constant, which is equal to 10.32; $n_{\rm s}$ refers to the 2DEG (two-dimensional electron gas) concentration at the hetero-interface. Figure 3(a) shows the characteristics of $n_{\rm s}$ versus $V_{\rm G}$. The relationship between the electric field and the gate bias voltage is shown in Fig. 3(b). The electric field will be used in the calculation and analysis of the leakage mechanism.

Figure 4 shows the $\ln(J_{\rm R}/T^2)$ vs. $E^{0.5}$ characteristics at 273 K to 473 K. According to Eq. (2), the $\ln(J_{\rm R}/T^2)$ vs. $E^{0.5}$ should satisfy a linear relationship with the slope $K_{\rm TE}$. Figures 4(a) and 4(b) show the measured data of W-gate and TiN-gate AlGaN/GaN HEMTs, which fits the straight line well at different temperatures. However, as shown in Fig. 4(c), the extracted $K_{\rm TE}$ values of TiN- and W-gate devices from the $\ln(J_{\rm R}/T^2)$ versus $E^{0.5}$ measurement are much larger than the theoretical result. For W-gate AlGaN/GaN HEMTs, the value of $\varepsilon_{\rm s}$ extracted from the slope of the fitting curve of $K_{\rm TE}$ with $T/1000$ is 0.76, which is much smaller than the reported values for GaN (5.35) and AlN (4.77).[12] Therefore, the thermionic emission (TE) is not the main leakage mechanism for W gate AlGaN/GaN HEMTs at low reverse bias voltage.

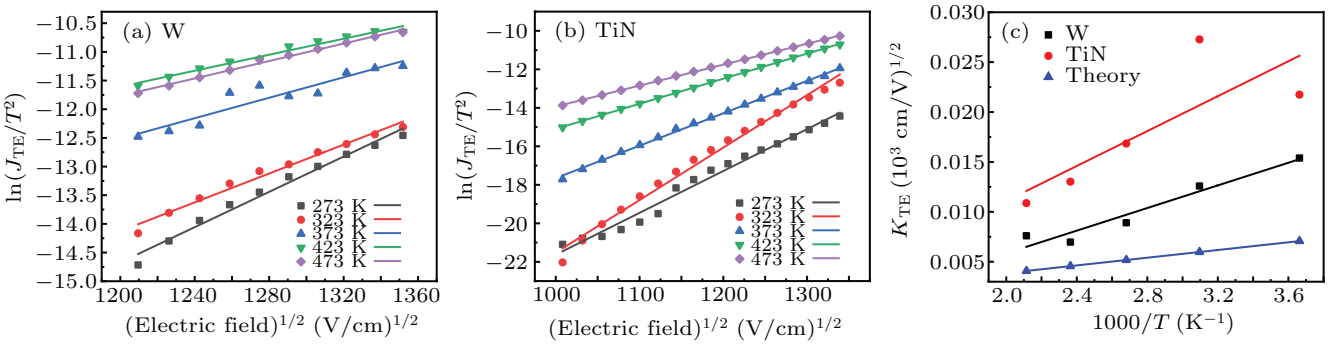


Fig. 4. (a) Behavior of $\ln(J_{\rm TE}/T^2)$ vs. $E^{0.5}$ and the linear fit to extract $K_{\rm TE}$ of W gate; (b) $\ln(J_{\rm TE}/T^2)$ vs. $E^{0.5}$ and the linear fit to extract $K_{\rm TE}$ of TiN gate; (c) $K_{\rm TE}$ measured from the reverse $J_{\rm R}$–$V_{\rm R}$ characteristics of W gate, TiN gate and calculated from the theoretical equation.

3.1.2. Poole–Frenkel emission current

In order to understand the gate leakage mechanism of AlGaN/GaN HEMTs in the low reverse bias region, the current density is plotted using the Poole–Frenkel emission (PF) emission model. PF emission refers to the carrier transport, which occurs through a trap state to the continuum states with the assistance of electric field. The PF current density $J_{\rm PF}$ is given by[12]

$$J_{\rm PF} = q n_0 \mu E \exp\left[-\frac{q}{k_{\rm B}T}\left(\varphi_{\rm t} - \sqrt{\frac{qE}{\pi \varepsilon_{\rm s(h)} \varepsilon_0}}\right)\right], \tag{6}$$

where μ refers to the electron mobility of AlGaN/GaN HEMTs; $q\varphi_{\rm t}$ refers to the effective barrier height for electron emission from a trapped state. Equation (6) can be rewritten as

$$\ln\left(\frac{J_{\rm PF}}{E}\right) = K_{\rm PF}(T)\sqrt{E} + C_{\rm PF}(T), \tag{7}$$

$$K_{\rm PF}(T) = \frac{q}{k_{\rm B}T}\sqrt{\frac{q}{\pi \varepsilon_{\rm s(h)} \varepsilon_0}}, \tag{8}$$

$$C_{\rm PF}(T) = \frac{q\varphi_{\rm t}}{k_{\rm B}T} + \ln(q n_0 \mu). \tag{9}$$

From Eq. (7), if the gate reverse leakage current is caused by PF, and then the curves of $\ln(J_{\rm PF}/E)$ versus $E^{0.5}$ will exhibit a linear relationship. Figures 5(a) and 5(b) are the experimental measurement curves of $\ln(J_{\rm PF}/E)$ versus $E^{0.5}$ in the temperature range from 273 K to 473 K for two devices with different gate materials. It can be clearly seen that the measured data for both devices still fit well with straight line. To further analyze the relationship between reverse leakage current and PF emission current, the $K_{\rm PF}$ data were extracted from the experimental measured curves at different temperatures and used to compare with the calculated theoretical values. As shown in Fig. 5(c), for W gate and TiN gate, the extracted $K_{\rm PF}$ data is much larger than the theoretical value, which indicate that the dominant leakage mechanism of W-gate and TiN-gate AlGaN/GaN HEMTs at low reverse bias voltages is not Poole–Frenkel emission. In addition, the $\varepsilon_{\rm s}$ values extracted from the slopes of the fitting curves of the $K_{\rm PF}$ vs. $1000/T$ are 2.96 (W)

and 2.02 (TiN), respectively, which are also inconsistent with the theory value (5.2) and the reported values of GaN (5.35) and AlN (4.77).[12]

On the other hand, C_{PF} can be extracted from Figs. 5(a) and 5(b). It can be seen from Fig. 5(d) that the C_{PF} of W gate is linearly fitted to $1000/T$, but the fitting effect of TiN gate is not good. In addition, the $q\varphi_t$ values of W gate and TiN gate extracted from Fig. 5(d) are 0.836 eV and 1.289 eV, respectively. The $q\varphi_t$ value extracted from W gate and TiN is much larger than the reported 0.17 eV–0.34 eV.[12,27] Therefore, Poole–Frenkel emission is not the principal leakage mechanism under low reverse bias voltage.

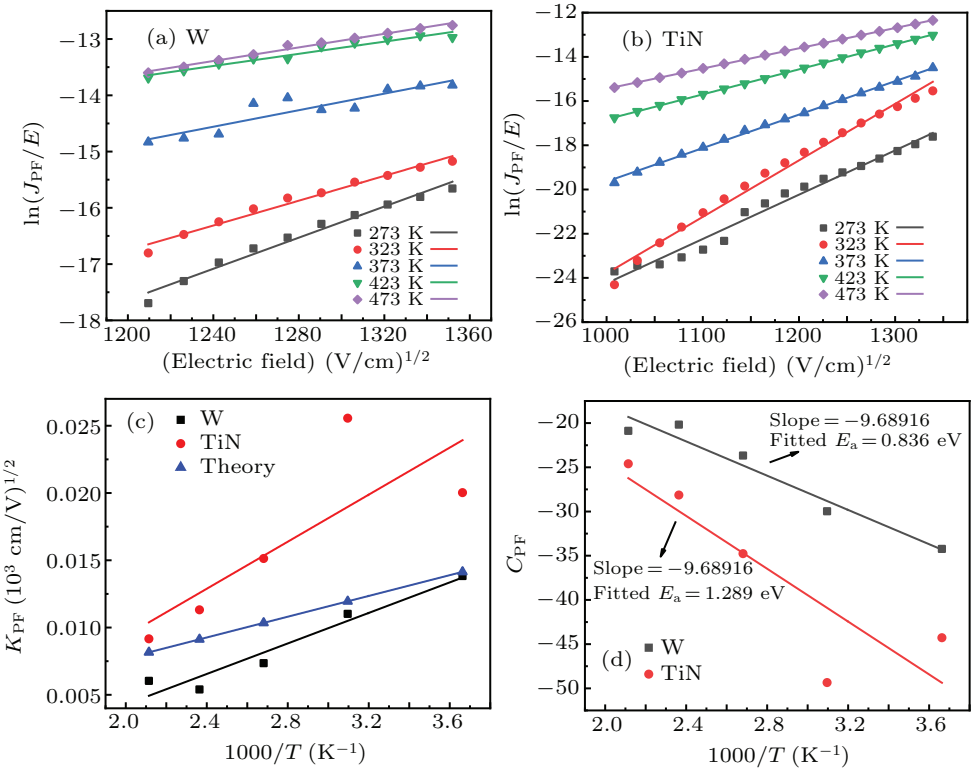


Fig. 5. (a) Characteristics of $\ln(J_{PF}/E)$ versus $E^{0.5}$ and the linear fit to extract K_{PF} of W gate; (b) $\ln(J_{PF}/E)$ versus $E^{0.5}$ and the linear fit to extract K_{PF} of TiN gate; [(c), (d)] K_{PF} and C_{PF} measured from the reverse J_R–V_R characteristics of W gate and TiN gate and calculated from the theoretical equation.

3.1.3. Trap-assisted tunneling current

Based on the above analysis and verification of TE and PF reverse gate leakage mechanisms, another leakage mechanism should exist for W-gate and TiN-gate AlGaN/GaN HEMTs. In low reverse-bias region, trap-assisted tunneling (TAT) current becomes important because it can compensate for non-zero PF current at zero bias. The TAT current density J_{TAT} is given by[20]

$$J_{TAT} \propto \exp\left(\frac{-8\pi\sqrt{2qm_n^*}}{3hE}\varphi_t^{3/2}\right), \tag{10}$$

where $q\varphi_t$ refers to the trap energy level, m_n^* refers to the conduction band effective mass, and h refers to the Planck constant.

Figure 6 shows the experimental measurement data of $\ln(J_{TAT})$ versus $1/E$ in the temperature range 273 K–473 K. It can be seen from Figs. 6(a) and 6(b) that the curves of $\ln(J_{TAT})$ versus $1/E$ exhibit linear relationship at low bias voltage and at different temperatures. This indicates that the leakage mechanism of AlGaN/GaN HEMTs with W gate and TiN gate under low reverse bias voltage is most likely the TAT-current mechanism. To further verify whether the leakage mechanism is TAT current, the trap energy level $q\varphi_t$, which is below the conduction bands edge, is extracted from the curves of the $\ln(J_{TAT})$ versus $1/E$ at different temperatures.

As shown in Fig. 7, $q\varphi_t$ decreases with the increasing temperature. The reason for this phenomenon is that the forbidden band will slightly shrink as the temperature increases, which reduces the trap energy levels $(q\varphi_t)$.[19] The extracted value of $q\varphi_t$ for W is smaller than that of TiN. For W, the value of $q\varphi_t$, extracted in region Ⅱ, i.e., at low reverse bias voltage $(-1.5 < V_R < 0$ V), is 1.51 eV–2.42 eV, which is close to the 1.7–2.3 eV reported by Liu *et al.*,[28] these values conform to the TAT mechanism. For TiN, the values of $q\varphi_t$ extracted at bias voltages $(-2.3$ V $< V_R < 0$ V) are 1.57 eV–2.93 eV, which is close to 1.8–2.45 eV reported by Liu *et al.*[13] Therefore, the leakage mechanism of AlGaN/GaN HEMTs with W gate and TiN gate under low reverse bias voltage is mainly the TAT mechanism.

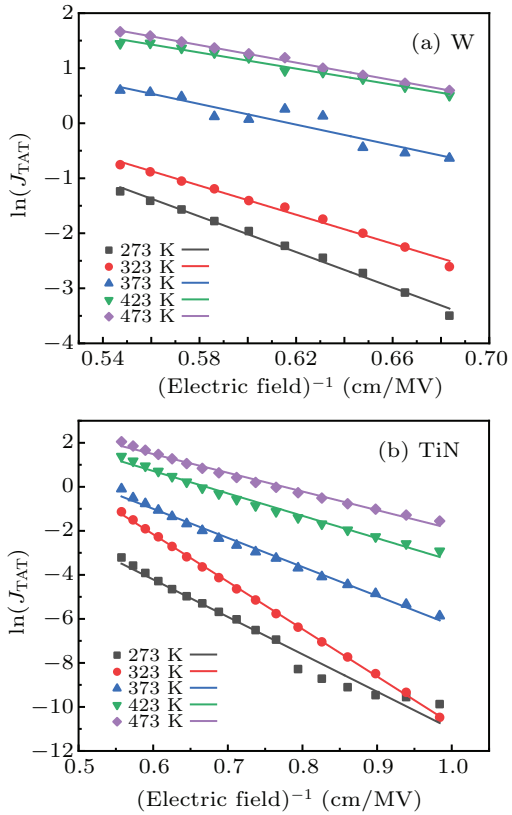


Fig. 6. (a) Characteristics of $\ln J_R$ of W gate versus $1/E$; (b) $\ln J_R$ of W and TiN gate versus $1/E$.

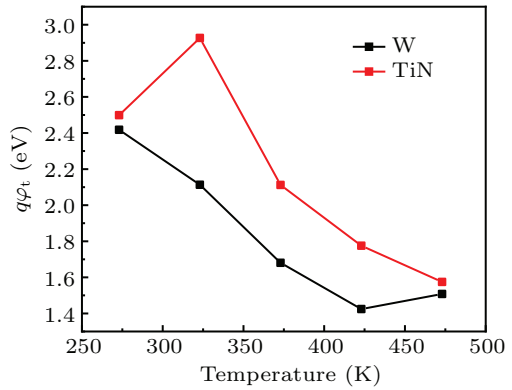


Fig. 7. The extracted $q\varphi_t$ of W gate and TiN gate at different temperatures and at low reverse bias voltage.

3.2. Leakage current mechanisms at high reverse bias voltage

The analytical results and discussion mentioned above indicate that AlGaN/GaN HEMTs using W-gate and TiN-gate have the same leakage mechanism at low reverse bias, which is the TAT-current mechanism. At high reverse bias voltage (in region I), with the reverse gate bias voltage ($V_R < V_{Th}$) further increased, the electric field across the barrier increases, which makes the tunnel barrier thinner so that the carriers can pass through the triangular barrier more easily. Therefore, the leakage mechanism under high reverse bias may be a tunneling mechanism, thus PF and TE mechanisms can be ruled out. The leakage mechanisms of Au-free gate AlGaN/GaN HEMTs under high reverse bias may include: Fowller–Nordheim tunneling (FN), two-dimensional variable ranging hopping (2D-VRH) mechanism, and thermally activated trap assisted tunneling (TAT).[29] It can be realized from the FN mechanism that when the temperature increases and the electric field strength increases, the reverse leakage current density should remain unchanged. However, as shown in Fig. 2, when the temperature increases and the electric field strength increases, the reverse leakage current continues to increase. Therefore, the Fowler–Nordheim tunneling (FN) mechanism can be excluded. By using a double-gate structure with a grid pitch of 4 μm and a grid width of 60 μm, the reverse surface leakage current can be accurately evaluated. The surface leakage current I_{surf} and bulk leakage current I_{bulk} of W-gate and TiN-gate AlGaN/GaN HEMTs are shown in Fig. 8. It can be clearly seen that the bulk leakage current I_{bulk} is much larger than the surface leakage current I_{surf}, at least 5–6 orders of magnitude larger. Therefore, the leakage mechanism is less likely to be surface leakage at high reverse bias gate voltage, more likely to activate the TAT mechanism.

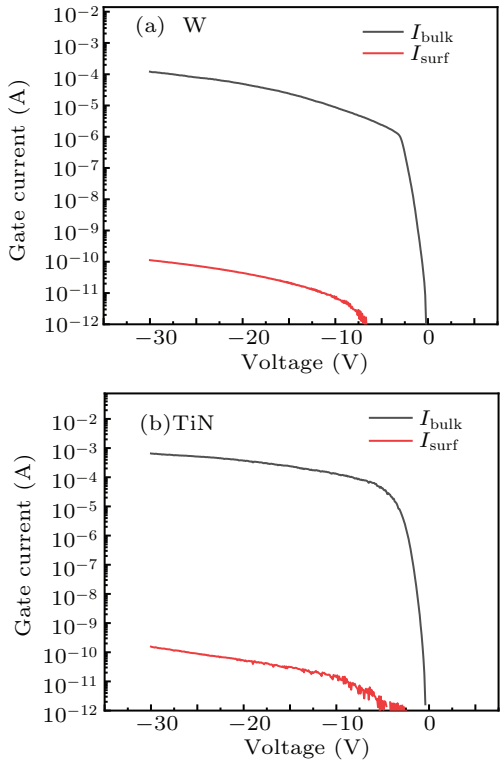


Fig. 8. Plots of reverse surface leakage current I_{surf} and bulk leakage current I_{bulk} versus voltage: (a) W gate AlGaN/GaN HEMT, (b) TiN gate AlGaN/GaN HEMT.

As shown in Fig. 2, the reverse leakage current density increases with the measurement temperature, which shows that it is related to the thermal activation process and can be expressed by[12,30]

$$J_R \propto \frac{qC_tN_t}{E}\exp\left(-\frac{E_a}{k_BT}\right), \tag{11}$$

$$\ln(J_{\rm R}) \propto -\frac{E_{\rm a}}{k_{\rm B}T}, \tag{12}$$

where E refers to the electric field at Schottky junction which is a constant according Eq. (5) and Fig. 3(b) at high reverse bias voltage. $C_{\rm t}$ refers to the trap energy dependent rate constant. $N_{\rm t}$ refers to the uniform trap concentration. T, $J_{\rm R}$, and $E_{\rm a}$ represent temperature, reverse saturation current density, and activation energy, respectively.

Table 2. The extracted activation energy of W-gate and TiN-gate AlGaN/GaN HEMTs at different reverse bias voltage.

Voltage (V)	W gate $E_{\rm a}$ (eV)	TiN gate $E_{\rm a}$ (eV)
–5	0.12688	0.20128
–10	0.08366	0.17385
–15	0.07140	0.14415
–20	0.06564	0.12652
–25	0.06379	0.11719
–30	0.05512	0.11170

As shown in Fig. 9, the $\ln J_{\rm R}$ vs. $1000/T$ curves of W-gate and TiN-gate AlGaN/GaN HEMTs can be fitted well with straight lines under different biases at various temperatures. At high reverse bias voltage, the electrons can easily obtain the activation energy $E_{\rm a}$ and are more likely to be emitted into the trap state. Figures 10(a) and 10(b) show the Arrhenius plot of the extracted activation energy ($E_{\rm a}$) from curves of $\ln J_{\rm R}$ vs. $1000/T$. Table 2 shows the $E_{\rm a}$ of W-gate and TiN-gate AlGaN/GaN HEMTs extracted under the different reverse bias voltages. For W gate, at $V_{\rm R} = -5$ V, and -15 V, the extracted $E_{\rm A}$ is 0.127 eV and 0.071 eV, respectively, which are close to 0.115 eV reported by Li *et al.*[12] For TiN gate, at $V_{\rm R} = -5$ V, and -15 V, the extracted $E_{\rm A}$ is 0.201 eV and 0.144 eV, respectively, which are close to 0.18 eV reported by Miller *et al.*[31] This further indicates that under high reverse bias conditions, thermally activated TAT is the main component of leakage current of W-gate and TiN-gate AlGaN/GaN HEMTs. In addition, it can be clearly seen that the extraction energy $E_{\rm a}$ of W-gate and TiN-gate AlGaN/GaN HEMTs decreases with increasing reverse bias voltage. This is mainly due to the increase of bias voltage that reduces the effective barrier height and thus reduces the energy required for electron tunneling barrier. This result is consistent with the data reported in Refs. [19,31]. As shown in Fig. 10(c), the $E_{\rm a}$ extracted from the W-gate and TiN-gate AlGaN/GaN HEMTs exhibits an exponential relationship with the bias voltage, which can be expressed as

$$E_{\rm a} = A\exp\left(-\frac{V_{\rm R}}{B}\right) + C, \tag{13}$$

where $V_{\rm R}$ refers to reverse bias voltage. A, B, and C are the related fitting parameters. For W-gate AlGaN/GaN HEMTs, A, B, and C are 0.168, 5.454, and 0.059, respectively. For TiN-gate AlGaN/GaN HEMTs, A, B, and C are 0.159, 14.01, and 0.09, respectively. The exponential relationship between $E_{\rm a}$ and reverse bias voltage is also consistent with that reported by Liang *et al.*,[19] which further suggests that leakage mechanism of W-gate and TiN-gate AlGaN/GaN HEMTs is thermally activated TAT at high reverse bias voltage. In addition, according to Fig. 2 and Table 1, it is also found that at the same temperature and gate voltage, the reverse leakage current of W-gate AlGaN/GaN HEMTs is smaller than that of TiN-gate AlGaN/GaN HEMTs at high reverse bias voltage ($V_{\rm R} < -5$ V). According to Eq. (11), this may be caused by the fact that the trap density of the TiN gate is greater than that of the W gate. Suzuki *et al.* reported the existence of a high density of traps near the metal-nitrided oxide interface region, which is attributed to nitrogen incorporated during the nitridation.[32] Therefore, extra traps may be generated in the area of Schottky contact due to nitridation during formation of TiN gate in the TiN gate AlGaN/GaN HEMTs compared to W gate AlGaN/GaN HEMTs. The leakage mechanism of conventional Ni/Au gate AlGaN/GaN HEMT with N_2 plasma surface treatment belongs to the Poole–Frenkel emission mechanism (PF) at low reverse bias and to the surface leakage mechanism at high reverse bias.[13] It can be seen that the leakage mechanism at both low and high reverse biases is different from W-gate and TiN-gate AlGaN/GaN HEMTs.

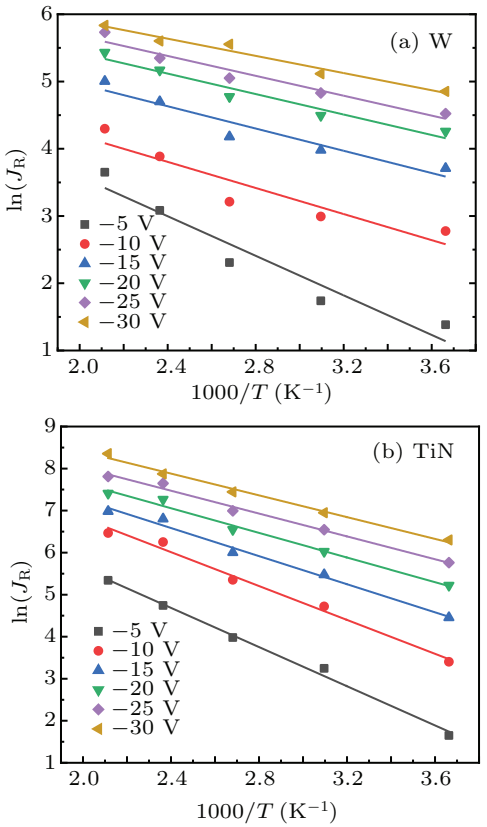


Fig. 9. (a) Characteristics of $\ln J_{\rm R}$ of W gate AlGaN/GaN HEMTs versus $1/E$, (b) $\ln J_{\rm R}$ of TiN gate AlGaN/GaN HEMTs versus $1/E$.

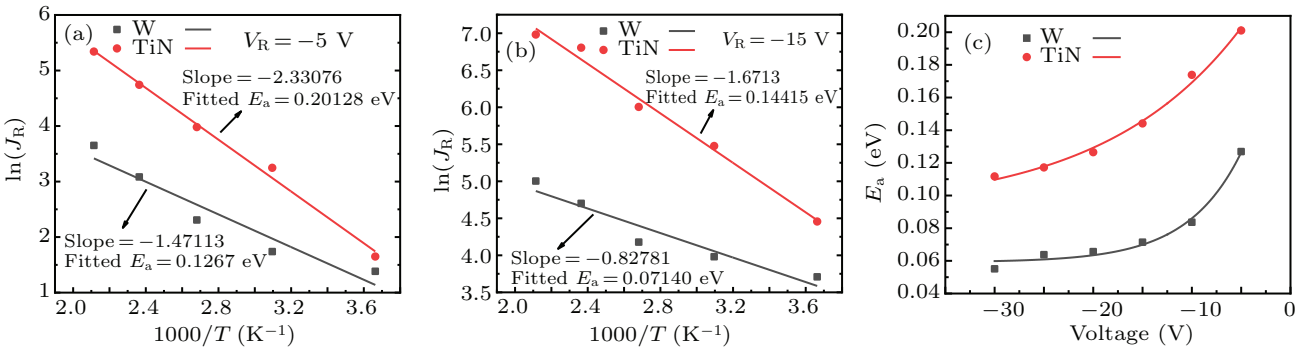


Fig. 10. (a) Characteristics of $\ln J_R$ of W gate and TiN gate AlGaN/GaN HEMTs vs. $1000/T$ at $V_R = -5$ V, (b) $\ln J_R$ of W gate and TiN gate AlGaN/GaN HEMTs vs. $1000/T$ at $V_R = -20$ V, (c) E_a of the two devices versus V_R.

4. Conclusion and perspectives

In summary, we have studied the reverse leakage current transmission mechanism of W-gate and TiN-gate AlGaN/GaN HEMTs. Through calculation and analysis, it is found that at temperatures of 273 K–473 K and in the entire reverse bias voltage range (-30 V $< V_R < 0$), the W gate and TiN gate AlGaN/GaN HEMTs with N_2 plasma surface treatment have the same leakage current mechanism, the main reverse leakage current mechanism is of TAT. In addition, it is also found that the reverse leakage current of W-gate AlGaN/GaN HEMTs is smaller than that of TiN-gate AlGaN/GaN HEMTs. The trap level $q\varphi_t$ is extracted. For W-gate AlGaN/GaN HEMTs, the values extracted at low bias voltage are in the range 1.33 eV–2.26 eV. For TiN gate AlGaN/GaN HEMTs, the values extracted at low bias voltage are 1.59 eV–3.08 eV. The activation energy E_a is extracted at high reverse bias voltage, and the values extracted by AlGaN/GaN HEMTs of W gate and TiN gate are 0.0551 eV–0.127 eV and 0.112 eV–0.201 eV, respectively.

Acknowledgement

The authors thank Kui Cheng for his help in measurement.

References

[1] Li L, Kishi A, Shiraishi T, Ying J, Wang Q, Ao J P and Ohno Y 2013 *Jpn. J. Appl. Phys.* **52** 11NH01
[2] Zheng X F, Fan S, Chen Y H, Kang D, Zhang J K, Wang C, Mo J H, Li L, Ma X H, Zhang J C and Hao Y 2015 *Chin. Phys. B* **24** 027302
[3] Johnson D W, Ravikirthi P, Suh J W, Lee R T P, Hill R J W, Wong M H, Piner E L and Harris H R 2014 *J. Vac. Sci. Technol. B* **32** 030606
[4] Peralagu U, Jaeger B D, Fleetwood D M, Wambacq P and Zhao S E 2019 *Proceedings of the* 2019 *IEEE International Electron Devices Meeting (IEDM)*, December 7–11, 2019, San Francisco, CA, USA, pp. 17.2.1–17.2.4
[5] Li Y, Ng G I, Arulkumaran S, Liu Z H, Ranjan K, Xing W C, Ang K S, Murmu P P and Kennedy J 2017 *Phys. Status Solidi A* **214** 1600555
[6] Soltani A, Rousseau M, Gerbedoen J C, Mattalah M, Bonanno P L, Telia A, Bourzgui N, Patriarche G, Ougazzaden A and Benmoussa A 2014 *Appl. Phys. Lett.* **104** 233506
[7] Lu C Y, Chang E Y, Huang J C, Chang C T, Lin M H and Lee C T 2008 *J. Electron. Mater.* **37** 624
[8] Shin J H, Park J, Jang S, Jang T and Kim K S 2013 *Appl. Phys. Lett.* **102** 243505
[9] Lee C S, Chang E Y, Chang L, Fang C Y and Huang J S 2003 *Jpn. J. Appl. Phys.* **42** 4193
[10] Zheng X F, Fan S, Kang D, Sun W W, Ma X H and Hao Y 2015 *Proceedings of the* 2014 *IEEE 12th International Conference on Solid-State and Integrated Circuit Technology, ICSICT*, October 28–31, 2014, Guilin, China, pp. 1–3
[11] Xu N, Hao R, Chen F, Zhang X, Zhang H, Zhang P, Ding X, Song L, Yu G and Cheng K 2018 *Appl. Phys. Lett.* **113** 152104
[12] Li Y, Ng G I, Arulkumaran S, Ye G, Liu Z H, Ranjan K and Ang K S 2017 *J. Appl. Phys.* **121** 044504
[13] Liu H, Zhang Z and Luo W 2018 *Solid-State Electron.* **144** 60
[14] Ha W J, Chhajed S, Oh S J, Hwang S, Kim J K, Lee J H and Kim K S 2012 *Appl. Phys. Lett.* **100** 132104
[15] Lee J M, Chang K M, Kim S W, Huh C, Lee I H and Park S J 2000 *J. Appl. Phys.* **87** 7667
[16] Saadat O I, Chung J W, Piner E L and Palacios T 2009 *IEEE Electron Device Lett.* **30** 1254
[17] Hwang I, Kim J, Choi H S, Choi H, Lee J, Kim K Y, Park J B, Lee J C, Ha J and Oh J 2013 *IEEE Electron Device Lett.* **34** 202
[18] Kawanago, Takamasa, Kakushima, Kuniyuki, Kataoka, Yoshinori, Nishiyama, Akira, Sugii, Nobuyuki, Wakabayashi, Hitoshi, Tsutsui, Kazuo, Natori, Kenji, Iwai and Hiroshi 2014 *IEEE Trans. Electron Devices* **61** 785
[19] Liang J, Lai L, Zhou Z, Zhang J, Zhang J, Xu J, Zhang Y, Liu X and Luo W 2019 *Solid-State Electron.* **160** 107622
[20] Liu Z H, Ng G I, Arulkumaran S, Maung Y and Zhou H 2011 *Appl. Phys. Lett.* **98** 163501
[21] Arslan E, Buetuen S and Ozbay E 2009 *Appl. Phys. Lett.* **94** 221906
[22] Wang A, Zeng L and Wang W 2017 *ECS J. Solid State Sci. Technol.* **6** S3025
[23] Yan D, Jiao J, Ren J, Yang G and Gu X 2013 *J. Appl. Phys.* **114** 144511
[24] Turuvekere S, Dasgupta A and Dasgupta N 2015 *IEEE Trans. Electron Devices* **62** 3449
[25] Ahmed N and Dutta A K 2017 *Solid-State Electron.* **132** 64
[26] Yan D, Lu H, Cao D, Chen D, Zhang R and Zheng Y 2010 *Appl. Phys. Lett.* **97** 153503
[27] Turuvekere S, Karumuri N, Rahman A A, Bhattacharya A, Dasgupta A and Dasgupta N J I T o E D 2013 *IEEE Trans. Electron Devices* **60** 3157
[28] Liu Z H, Ng G I, Zhou H, Arulkumaran S and Maung Y K T 2011 *Appl. Phys. Lett.* **98** 113506
[29] Yua S M, Guan X M and H S Philip Wongb 2011 *Appl. Phys. Lett.* **99** 063507
[30] Sathaiya D M and Karmalkar S 2008 *IEEE Trans. Electron Devices* **55** 557
[31] Miller E J, Yu E T, Waltereit P and Speck J S 2004 *Appl. Phys. Lett.* **84** 535
[32] Suzuki E, Schroder D K and Hayashi Y 1986 *J. Appl. Phys.* **60** 3616